Journal of Physics: Conference Series

The use of segregated heat sink structures to achieve enhanced passive cooling for outdoor wireless devices

To cite this article: K O'Flaherty and J Punch 2014 *J. Phys.: Conf. Ser.* **525** 012019

The use of segregated heat sink structures to achieve enhanced passive cooling for outdoor wireless devices

K O'Flaherty, J Punch
CTVR, Stokes Institute, University of Limerick, Limerick, Ireland.

Email: kevin.oflaherty@ul.ie

Abstract. Environmental standards which govern outdoor wireless equipment can stipulate stringent conditions: high solar loads (up to 1 kW/m^2), ambient temperatures as high as 55ºC and negligible wind speeds (0 m/s). These challenges result in restrictions on power dissipation within a given envelope, due to the limited heat transfer rates achievable with passive cooling. This paper addresses an outdoor wireless device which features two segregated heat sink structures arranged vertically within a shielded chimney structure: a primary sink to cool temperature-sensitive components; and a secondary sink for high power devices. Enhanced convective cooling of the primary sink is achieved due to the increased mass flow within the chimney generated by the secondary sink. An unshielded heat sink was examined numerically, theoretically and experimentally, to verify the applicability of the methods employed. Nusselt numbers were compared for three cases: an unshielded heat sink; a sink located at the inlet of a shield; and a primary heat sink in a segregated structure. The heat sink, when placed at the inlet of a shield three times the length of the sink, augmented the Nusselt number by an average of 64% compared to the unshielded case. The Nusselt number of the primary was found to increase proportionally with the temperature of the secondary sink, and the optimum vertical spacing between the primary and secondary sinks was found to be close to zero, provided that conductive transfer between the sinks was suppressed.

1. Introduction

The recent increase in demand for mobile data has presented significant challenges for contemporary wireless communications systems. Active antenna arrays, remote radio heads, pico- and femto- cells are typical artefacts of today's wireless communication infrastructure. These devices are subject to substantial packaging restrictions, strict reliability requirements, severe environmental conditions, the imperative of passive cooling, strict constraints on weight (~15-20 kg) and volume, and strict Ingress Protection (IP) ratings. Furthermore, environmental standards which govern outdoor wireless equipment stipulate stringent conditions: high solar loads (up to 1 kW/m^2), ambient temperatures as high as 55ºC and negligible wind speeds (0 m/s) [1]. These challenges impose limitations on the power dissipation within a given envelope, as a consequence of the limited heat transfer rates achievable with passive cooling. Most contemporary outdoor wireless artefacts feature a cast metal casing which serves as a heat sink: moreover, most wireless artefacts feature two broad classes of device, each with different thermal characteristics: relatively low power, temperature-sensitive devices such as logic ICs; and high power devices such as Power Amplifiers (PAs) which can reliably tolerate high operating temperatures. These two classes of device may be segregated on to different assemblies on account of their function, and they may also be separated in terms of their heat sinking – for example, on opposing sides of a cast 'clamshell' structure. Finally, some outdoor equipment also features shields to mitigate solar ingress, which can act to induce conditions of chimney flow over the casing.

The configuration under investigation in this paper features two conventional heat sink structures within a shield that acts to induce chimney flow. Bar-Cohen and Rohsenow [2] investigated heat sinks as a series of vertical parallel plates under conditions of constant heat flux and constant temperature, and proposed a correlation for the Nusselt number which revealed an optimum fin spacing. Malhammer [3] built upon this correlation, incorporating the effect of the base plate on the optimum spacing. Shabany [4] developed relations for the view factor of a plate-fin heat sink. Khor *et al.* [4] experimentally investigated these relations for thermal radiation and view factor of plate-fin heat sinks. The use of a chimney structure to enhance flow is not uncommon; one of the earliest works by Moore [5] examined a natural draft heat exchanger system for large dry cooling towers. Lee and Yan [6] investigated laminar natural convection for an unheated entry and unheated exit with a heated middle section; they found that the induced volume flow rate increased with both decreasing unheated entry length and increasing total length of heated and unheated exit. Naylor and Tarasuk investigated numerically [7] and experimentally [8] a divided vertical channel with heated walls on the chimney and a heated dividing plate. The position of the divided plate, relative to the inlet, strongly influenced the heat transfer rate at lower Rayleigh numbers. The average Nusselt number for a plate at the inlet was nearly double that for a plate located at the exit. Fischer *et al.* [9] formulated an analytical solution for a natural convection draft heat sink system, based on previous experimental work. A porosity term was used to capture effects from a wider chimney and to account for the potential reduction in mean velocity at the exit and the mean channel velocity. It was found that a reduction in heat sink height can be compensated by higher local heat transfer rates induced by the chimney effect; achieved by a large temperature (and thus density) difference between the fluid inside and outside the chimney.

The preceding literature review indicates the potential to utilize a chimney structure to enhance heat transfer; however the use of multiple independently placed heat sinks is rare. This paper aims to address the potential to utilize two segregated heat sink structures arranged vertically within a shield or chimney structure: a lower, or primary, sink to cool temperature-sensitive components; and an upper, or secondary, sink for the high power components which can tolerate higher temperatures. Enhanced convective cooling of the primary sink is achieved due to the increased mass flow within the chimney generated by the secondary sink. The specific practical focus of the paper is the improvement of heat dissipation in a representative remote radio head by exploiting the chimney effect and a secondary segregated structure. Experimental details are presented in the following section.

2. Experimentation

Two identical heat sinks, representative of a typical remote radio head, were machined in aluminium 6082T6 to the dimensions listed in table 1 and illustrated in figure 1.

Table 1: Dimensions of the heat sink structure and shield.

Term	Value
Width, W	149.5 mm
Length, L	300.0 mm
Height, H	60.0 mm
Fin thickness, t	1.9 mm
Base thickness, B	20.0 mm
Fin spacing, S	11.5 mm
No. fins, N (one side)	12
Hole spacing, L_{h1}	25.0 mm
Hole spacing, L_{h2}	50.0 mm

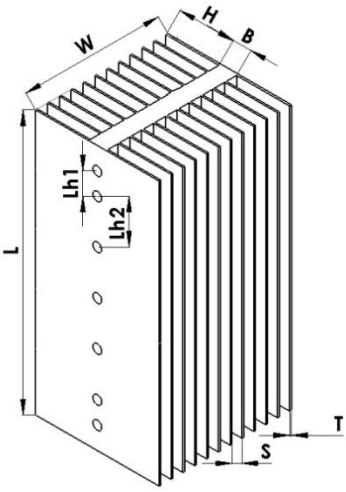

Figure 1: Dimensions of the heat sink.

Seven 10mm diameter, 150mm long cartridge heaters, each coated in thermal paste with a nominal thermal conductivity of 0.67 W/m.K, were embedded into the base plate of each heat sink. The sinks were double-sided (fins both sides of the base plate) in order to obviate errors due to losses from the back plate of a single-sided sink structure. In addition, the sinks were anodized black to ensure a known emissivity to accurately quantify radiative losses. Three different configurations were tested, as shown in figure 2; a single heat sink with no shield (unshielded); a single heat sink within a shield (chimney); and two heat sinks in a shield (segregated structure, primary and secondary). The shield, which was made from polycarbonate, featured a length of 900mm, width of 161mm, thickness of 5mm, and clearance of 5.75mm from the surfaces of the sink. The shield cover neither the top nor bottom of the heat sink, in order to allow air to flow freely through the sink. All testing was carried out in a polycarbonate enclosure, five times the length of the heat sink, to reduce uncertainties due to air currents in the laboratory. The segregated structure was further investigated by quantifying the impact of the gap distance on heat transfer from the primary heat sink, as shown in figure 3.

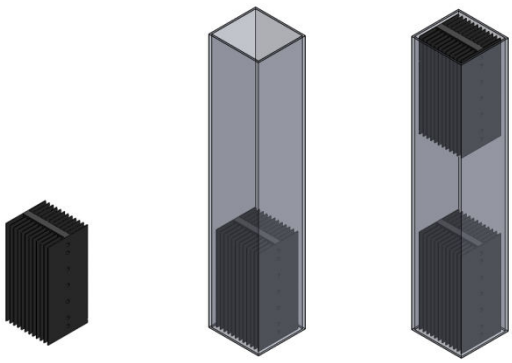

Figure 2: The three different configurations under consideration: unshielded (left), shielded (centre) and segregated (right).

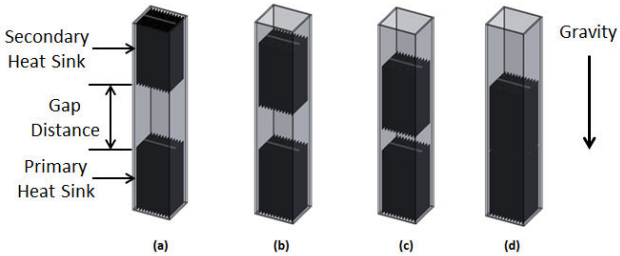

Figure 3: Segregated heat sink structures with varied heat sink gap; (a) 300mm (b) 200mm, (c) 100mm and (d) 5mm.

To enable the quantification of radiative losses, a thermocouple probe was attached to the heat sink at a range of locations and monitored at different temperatures using a FLUKE Ti32 handheld thermal imager. The emissivity of the heat sink was calculated using a process outlined in Khor *et al.* [4], and found to have an average value of 0.97. The polycarbonate had an emissivity of 0.95.

Temperature was monitored using National Instruments TBX-68T and USB-TC01 cards reading K-type thermocouples, calibrated to ±0.1℃, placed in different locations and depths within the base of the heat sink. The average temperature of the base plate of the heat sink was used to calculate values for Nusselt number, Elenbaas number and the film temperature. Three power supplies – a BSI PSM 3/2A, a Sorensen DCS 80-37 and a Delta Elektronika SM 3004-D – were used to provide controlled voltage to each cartridge heater. Equation (1) was used to calculate the power dissipated. Labview 2011 provided PID control to each individual heater, using feedback from a thermocouple to vary the duty cycle of a pulse-width modulated digital output. A National Instruments PCI-6229 card and a CB-68LP connector block generated the pulse-width modulated digital output which switched a Crydom D2D07 relay on and off.

$$P = \sum V_h \frac{V_r}{R} \tag{1}$$

The voltage drop across the heaters (V_h) and the average voltage drop in each resistor (V_r) were measured using a calibrated FLUKE 8842a multimeter, connected as close as possible to the cartridge heater, and a National Instruments PCI-6229 card with a CB-68LP connector block to record the average voltage drop in each resistor (V_r), of known resistance (R), connected in series with each heater. A circuit diagram for three heaters and resistors is shown in Figure 4. V_r was averaged over a 10 minute period after the system reached thermal equilibrium.

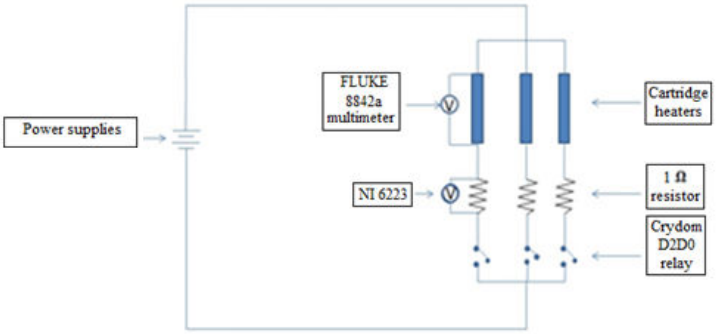

Figure 4: Schematic of the electrical setup.

The Nusselt number was calculated by removing radiation heat dissipation, calculated using the relations presented in section 3.2, to isolate convective dissipation in order to obtain an average heat transfer coefficient. The primary sink was maintained at a constant temperature of 25°C above ambient during the experimentation, while the temperature of secondary heat sink was increased sequentially above the temperature of the primary heat sink. The method of Kline and McClintock [10] was used to conduct an uncertainty analysis on the measured data. The maximum uncertainty in Nusselt number was found to be 8.2%, with most cases below this value.

3. Theory

Theoretical models, using established literature, were used to quantify the radiative and convective heat transfer from an unshielded heat sink with the characteristic dimensions of the remote radio head defined in section 2. The heat sink was optimized at an operating temperature of 80°C in an ambient temperature of 55°C, as stipulated by a commonly-used industry standard [1].

3.1. Convective heat transfer

The convective heat transfer from a heat sink approximated as a series of parallel plates is governed by the Rayleigh number (Ra_L) based on the length of the heat sink (L):

$$Ra_{\mathrm{L}} = \frac{g\beta(T_s - T_{amb})L^3}{\gamma^2} Pr \tag{2}$$

Where g is acceleration due to gravity (~9.81m/s^2) and the properties of air are as follows: the expansivity, β (K^{-1}); the kinematic viscosity, ν (m^2/s); and Prandtl number, Pr (-). The plates are assumed to be at a uniform temperature T_s in an ambient of temperature T_{amb}. For heat sink structures, the Rayleigh number can be modulated by fin spacing, S, to yield the Elenbaas number:

$$El_{\mathrm{S}} = Ra_{\mathrm{L}}(S^4/L^4) \tag{3}$$

Equation (4) [11] is used to calculate the optimum spacing for the parallel plates of a heat sink, with equation (5) [3] applied to incorporate the influence of the base plate:

$$S_{\mathrm{opt}} = 2.71\left(\frac{Ra_L}{L^4}\right)^{-\frac{1}{4}} \tag{4}$$

$$S_{opt} = \frac{2\mathrm{HS}}{2\mathrm{H} + \mathrm{S}} \tag{5}$$

The optimum spacing (S_{opt}) for parallel plates is modified in equation (5) to a revised spacing (S) for a finned heat sink with a fin height (H). The convective heat transfer for an unshielded heat sink can be determined using equation (6) [2]:

$$Q_{conv} = NQ_{fin} + \overline{h_{base}}A_{\mathrm{base}}(T_s - T_{amb}) \tag{6}$$

The total heat removed by convection (Q_{conv}) is a sum of the number of fins (N) times the heat dissipation in a single fin (Q_{fin}), calculated using equation (8), and a base plate dissipating heat via

convection. The heat dissipated from the base plate is calculated using the heat transfer coefficient ($\overline{h_{base}}$), evaluated using equation (7), for the unfinned base area (A_{base}):

$$\overline{h_{base}} = 0.59\text{Ra}_{\text{L}}^{0.25}\frac{k_f}{L} \tag{7}$$

The heat transfer coefficient is calculated using the thermal conductivity (k_f) of the air at the film temperature and the Rayleigh number. The heat dissipation from a single fin is as follows:

$$Q_{fin} = \overline{h_{fin}}A_{fin}(T_s - T_{amb}) \tag{8}$$

The average Nusselt number ($\overline{Nu_S}$) over the finned surface of the heat sink is calculated using the Rayleigh number referenced to fin spacing (Ra_S), and the fin efficiency (η_{fin}), calculated using equation (10). This Nusselt number yields the heat transfer coefficient over the surfaces of the fin:

$$\overline{Nu_S} = \left[\frac{576}{\left(\frac{\eta_{fin}Ra_S S}{L}\right)^2} + \frac{2.87}{\left(\frac{\eta_{fin}Ra_S S}{L}\right)^{0.5}}\right]^{-0.5} = \frac{\overline{h_{fin}}S}{k_f} \tag{9}$$

Finally, the fin efficiency is calculated from Incropera *et al.* [12]:

$$\eta_{fin} = \frac{\tanh(aL_{\text{c}})}{aL_{\text{c}}} \tag{10}$$

Where the fin parameter, $m = \left(2\overline{h_{fin}}/k_{fin}\,t\right)^{1/2}$ and the corrected fin length, $L_{\text{c}} = L + (t/2)$.

3.2 Radiative heat transfer

An established model expressed in Shabany [13] was used to quantify the effects of radiation in order to isolate the convective heat dissipation in the experimental data:

$$Q_{rad} = \eta_{fin}\left(Q_{top} + Q_{bot} + Q_{side} + (\text{N} - 1)Q_{channel}\right) \tag{11}$$

The total heat removed by radiation (Q_{rad}) is calculated as the contributions from the top (Q_{top}), bottom (Q_{bot}), side (Q_{side}) and channel ($Q_{channel}$) surfaces. N is the number of fins and η_{fin} accounts for the temperature variation in the fins:

$$Q_{top} = Q_{bot} = \sigma\varepsilon(HtN + BW)(T_s^4 - T_{amb}^4) \tag{12}$$

$$Q_{side} = \sigma\varepsilon(4H + 2B + tN)L(T_s^4 - T_{amb}^4) \tag{13}$$

The heat dissipated by radiation from the top, bottom and side are evaluated using the Stefan-Boltzmann constant (σ), the base (T_s) and ambient (T_{amb}) temperatures, the emissivity (ε) of the heat sink, the fin height (H), fin thickness (t), base thickness (B), heat sink width (W), length (L) and number of fins (N).

$$Q_{channel} = \sigma\hat{F}(S + 2H)L(T_s^4 - T_{amb}^4) \tag{14}$$

The heat removed by radiation from each channel is a function of the channel gray body shape factor ($\hat{F}$) which is a function of F_{s-surr}, the total view factor between the walls and base of the channel and their surroundings:

$$\hat{\text{F}} = \frac{1}{((1-\varepsilon)/\varepsilon) + (1/F_{s-surr})} \tag{15}$$

$$F_{s-surr} \approx 1 - \frac{2(H/S)\left[(1 + (L/S)^2)^{1/2} - 1\right]}{2(H/S)(L/S) + [(1 + (L/S)^2)]^{1/2} - 1} \tag{16}$$

It should be noted that the fin efficiency values used in the convective and radiative calculations in this paper were found to be close to unity, as would be expected for a passively cooled heat sink.

4. Numerical modelling

In order to complement the experimental data, numerical modelling was performed using Star-CCM+ v6.02.007 from CD-adapco, running on a 64-bit Windows 7 PC. The modelling was used to examine the influence of two parameters associated with the segregated structure: the vertical spacing between the primary and secondary heat sinks, and the fin count of the secondary heat sink. In all cases, the heat sink and shield combinations, outlined in section 2, were modelled as a constant density, three-dimensional structure with segregated solid energy and surface-to-surface grey thermal radiation. The air was modelled as a three dimensional, laminar flow using constant density and invoking the Boussinesq approximation. Steady-state conditions were assumed throughout.

The heat sink, shown in figure 1, was represented with an emissivity of 0.968, thermal conductivity of 180W/m.K and density of $2700\,\mathrm{kg/m^3}$. The shielding material was made from polycarbonate with an emissivity of 0.953, conductivity of 0.19W/m.K and density of $1200\,\mathrm{kg/m^3}$. The numerical analysis used values obtained experimentally for the ambient temperature and the temperature difference. The properties of air were taken at the film temperature using values interpolated from table 3.

In the analysis presented in this paper, a fixed temperature difference above ambient is imposed on the heater locations, shown as L_{h1} and L_{h2} in figure 1. The simulation monitored heat dissipation of the heat sink and the maximum exit velocity from the primary heat sink. The solution criteria required the maximum velocity to have a standard deviation of less than 0.003m/s over 50 samples and the heat dissipation to be less than 0.05W in 100 samples. The meshing was checked against experimental values obtained by Oosthuizen [14] to ensure the simulation results were mesh independent.

Firstly, a single heat sink was numerically simulated in isolation and compared to experimental data and established correlations. The heat sink was then modelled at the base of a shield, 900mm in length, and simulated using the ambient temperatures and temperature difference listed in table 2. An unheated secondary heat sink was then added to the shielded structure, at the top of the shielded structure as shown in figure 2.

Table 2: Ambient temperature and temperature difference for an unshielded, shielded and secondary heat sink with no heat.

Unshielded		**Shielded**		**Secondary No Heat**	
Ambient (°C)	$\boldsymbol{T_p - T_\infty}$ (°C)	**Ambient** (°C)	$\boldsymbol{T_p - T_\infty}$ (°C)	**Ambient** (°C)	$\boldsymbol{T_p - T_\infty}$ (°C)
19.2	5.1	17.0	5.1	17.9	5.1
19.1	10.0	17.1	10.1	18.7	10.1
19.1	15.0	17.0	15.0	18.8	15.0
19.2	20.0	16.3	20.0	19.2	20.0
19.3	25.0	16.8	25.0	19.2	24.9
19.4	34.9	17.2	34.9	16.4	34.8
19.4	44.8	17.6	44.8	19.2	44.8
20.3	54.8	18.1	54.7	17.6	54.8
20.5	64.7	18.4	64.5	18.7	65.4

A heated secondary heat sink, temperature given in table 3, was numerically calculated at a primary-secondary spacing of 0mm up to 300mm in steps of 50mm; in addition, a spacing of 5mm was also evaluated. At a gap distance of 0mm, both heat sinks were in physical contact, however, they were not permitted to conduct heat to each other. The primary heat sink was maintained at a temperature difference of 24.9°C above ambient throughout.

Finally, based on the results from the location of the heated secondary heat sink, the number of fins on the secondary heat sink was varied. The fin thickness was kept constant while the number of fins was varied from 2, in steps of 2, up to 14 fins; additional variants with 7, 13 and 15 fins were tested. The thermal properties were evaluated at an ambient temperature of 19.5℃, a primary heat sink temperature of 25.0℃ above ambient and a secondary heat sink temperature of 64.4℃.

Table 3: Thermal properties of a heated secondary heat sink.

Secondary Heat Sink		
Gap Distance (mm)	**Ambient (℃)**	$T_{sec} - T_{\infty}$ (℃)
0	19.5	64.4
5	14.8	64.3
50	19.5	64.4
100	20.8	64.2
150	19.5	64.4
200	15.4	64.3
250	19.5	64.4
300	19.5	64.4

5. Results and discussion

Section 5 is split into three sub-sections which address, respectively: 5.1, the unshielded heat sink; 5.2, the shielded heat sink (within the chimney); and, 5.3, the segregated structure. For the segregated structure, a Nusselt ratio – a comparison against the baseline case of the unshielded heat sink – is also presented with a heated secondary heat sink present. The influences of the spacing between the primary and secondary heat sinks, and the fin count of the secondary sink, are also investigated.

5.1. Unshielded

Correlated, numerical and experimental values for the Nusselt number of the primary heat sink are plotted as a function of the Elenbaas number in figure 5. Error bars represent the uncertainty in the experimental values, which exhibited maxima of 9% and 7% respectively in the Nusselt and Elenbaas numbers. The experimental and numerical values are within 10% and 6% of the correlation values respectively, an indication of the adequacy of the investigative methods used in this paper.

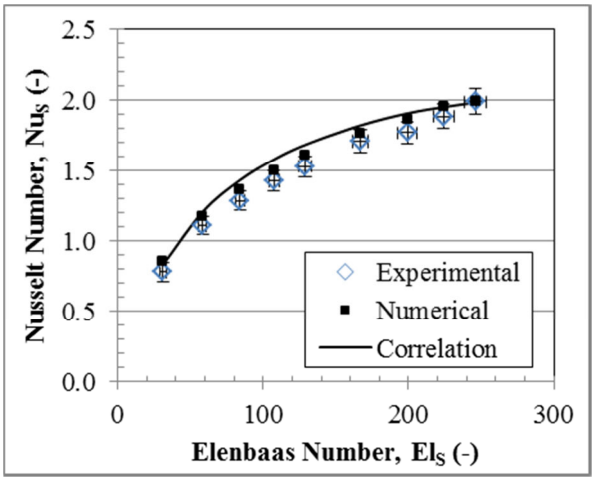

Figure 5: Nusselt Number as a function of Elenbaas Number for a single unshielded heat sink.

5.2. Chimney structure

Figure 6 presents the Nusselt number as a function of Elenbaas number for a shielded and an unshielded heat sink. The unshielded values are the numerical values presented in figure 5. The experimental and numerical values for a shielded heat sink agree within 8% of one another. The use of a shield augments the convective heat transfer by an average of 64% in comparison with an unshielded sink. At lower Elenbaas numbers, the shielded structure offers the most improvement, greater than 70%, however as the Elenbaas number increases, the enhancement diminishes to below 58%.

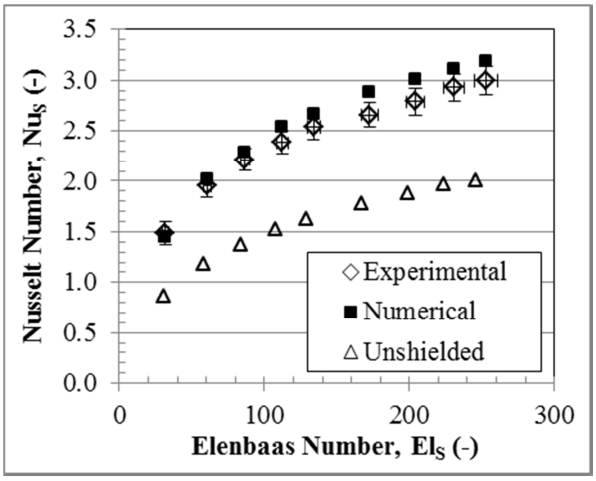

Figure 6: Nusselt number as a function of Elenbaas number for a shielded heat sink.

5.3. Secondary segregated structure

Figure 7 presents the numerical (squares) and experimental (diamond) Nusselt-Elenbaas data for a segregated structure with an unheated secondary heat sink. For comparison, numerical results for an unshielded (triangles) and a shielded (crosses) heat sink, replicated from figure 6, are also presented. A reduction of greater than 30% in Nusselt number in comparison with a shielded case is evident, however the addition of an unheated secondary heat sink in a shielded structure still outperforms an unshielded sink. The additional flow resistance offered by the secondary sink within the shield evidently diminishes the Nusselt number of the primary heat sink.

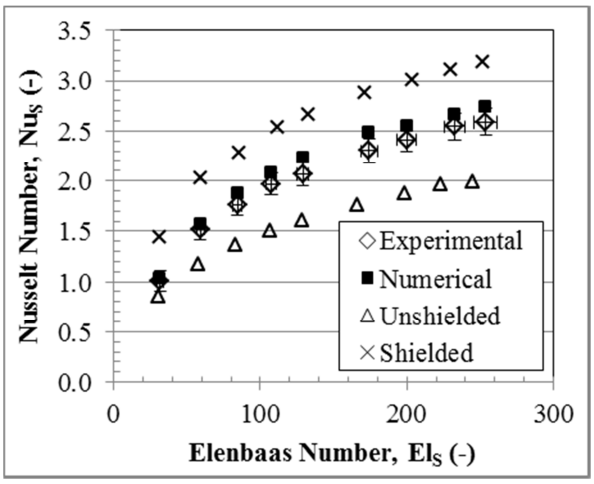

Figure 7: Nusselt number as a function of Elenbaas number for a secondary segregated structure with an unheated secondary heat sink.

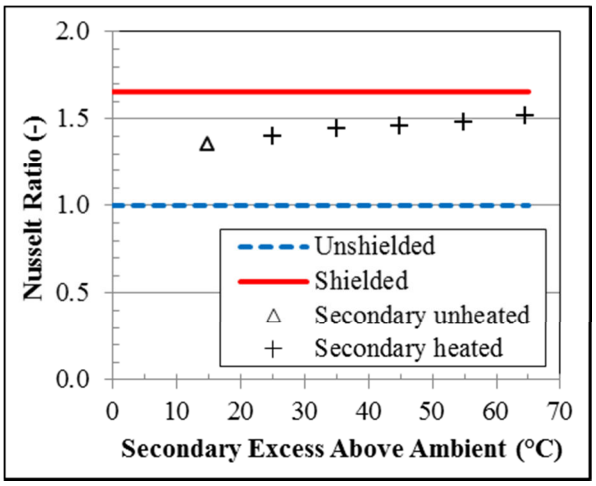

Figure 8: Experimental Nusselt ratio for a primary heat sink plotted against the secondary heat sink temperature excess over ambient.

In figure 8, the Nusselt ratio – a comparison against the baseline case of the unshielded heat sink – is plotted as a function of the base plate temperature of the secondary heat sink for four cases: unshielded, shielded, unheated secondary; and heated secondary. The Nusselt ratio exhibits an apparently linear increase in proportion to the temperature of the secondary heat sink, due to the additional mass flow induced by the secondary sink. At a secondary sink temperature of 65°C above ambient, the limit of the variable under consideration in this paper, an enhancement in the Nusselt number of ~50% was observed in comparison with the baseline unshielded sink. This finding has practical utility: there is an evident advantage in segregating heat sinks within a representative outdoor wireless device to carry temperature sensitive and power devices on primary and secondary heat sinks, within a shielded structure that promotes chimney flow.

Figure 9 presents the Nusselt ratio, based on numerical data, as a function of the spacing between the primary and secondary heat sinks. The secondary sink is fixed at a 65°C over ambient throughout, but an unheated secondary configuration (at 300mm spacing) is also included for reference. Baseline cases of unshielded (blue dashed line) and shielded (red solid line) are also presented. The idealised case of the secondary heat sink touching, but not conducting heat to, the primary heat sink provides an increase of over 75% in the Nusselt ratio. A spacing of 50mm provides the largest improvement for a practical scenario, surpassing the Nusselt ratio of a single heat sink within a shield.

Nusselt ratio, evaluated numerically, is presented in Figure 10 as a function of the number of fins of the secondary heat sink. Numerical data for an unshielded sink, a shielded sink and a segregated structure with an unheated secondary heat sink are also shown, each with 12 fins on each side (24 in total). The optimum fin count for the secondary heat sink was found to be 8, which would appear to be a counterintuitive finding (the form of equation 4 would suggest that the higher the temperature of a sink, the smaller the optimum spacing). However, the analysis presented here considers the behaviour of the primary heat sink in a segregated ensemble: moreover, the local air temperature at the inlet to the secondary sink is considerably higher than ambient, due to the influence of the primary sink.

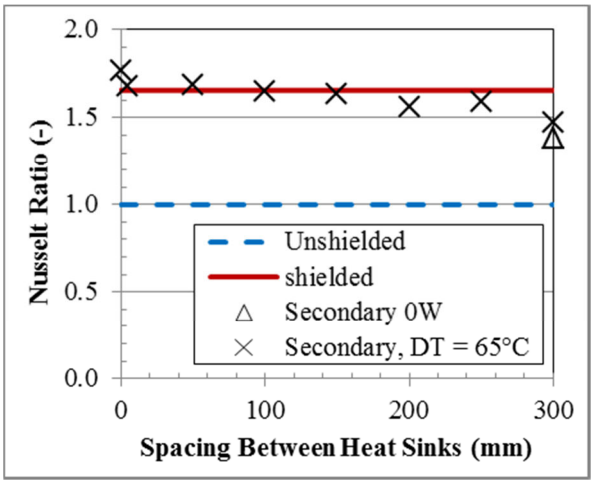

Figure 9: Nusselt ratio as a function of the spacing between the primary and secondary heat sinks.

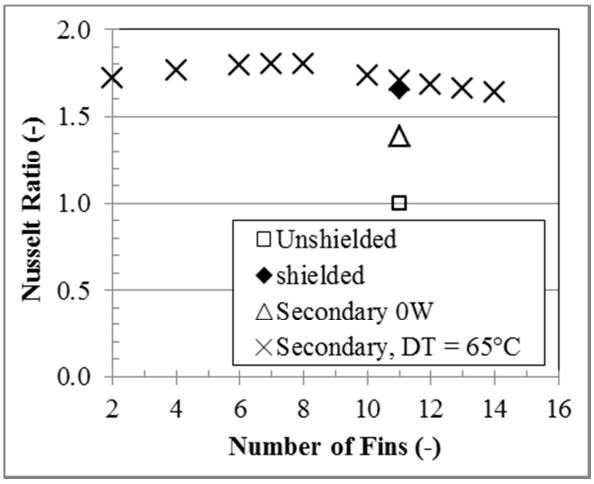

Figure 10: Nusselt ratio as a function of the number of fins on the secondary heat sink with a fixed primary-secondary spacing of 50mm.

6. Conclusions

In this paper, heat sink geometries representative of a remote radio head were examined in terms of the enhancement in the Nusselt-Elenbaas behaviour of the primary sink. The following improvements were found when compared to the Nusselt number of an unshielded heat sink:

- A single heat sink, when placed at the inlet of a shield three times its length, enhanced the Nusselt number by an average of 64% compared to the unshielded case.

- A segregated structure, with an unheated secondary heat sink, reduces the Nusselt number of the primary sink by over 30% compared to a shielded heat sink. The Nusselt number of the primary sink increases in proportion to the temperature of the secondary heat sink.
- The vertical spacing between primary and secondary heat sinks within a segregated structure could be adjusted to achieve further enhancements in the Nusselt number of the primary heat sink. The optimum location was found to occur at zero spacing, but this required the suppression of conduction between the sinks. Consequently, a spacing of ~50mm represented a practical choice.
- Variations of the number of fins on the secondary heat sink at a fixed temperature excess of 65℃ above ambient, in a segregated structure with 50mm primary-secondary spacing, offered an enhancement of 80% compared to an unshielded sink. The maximum enhancement occurred at 8 fins, resulting in a fin spacing of 19.2 mm.

In conclusion, the outcome of this paper is an improved understanding of a novel passive thermal management solution which is of practical relevance for the design of passively-cooled outdoor wireless communication equipment.

Acknowledgements
The authors acknowledge the financial support of Science Foundation Ireland under Grant No. 10/CE/I1853.

References

[1] Telcordia Technologies, "Generic Requirements for Electronic Equipment Cabinets," *GR-487-CORE,* no. 3, 2009.

[2] A. Bar-Cohen and W. M. Rohsenow, "Thermally optimum spacing of vertical, natural convection cooled, parallel plates," *Journal of Heat Transfer,* no. 106, pp. 116-123, 1984.

[3] A. Malhammer, "Optimum Sized Air Channels for Natural Convection Cooling," in *Telecommunications Energy Conference*, Stockholm, 1987.

[4] Y. K. Khor, Y. M. Hung and B. K. Lim, "On the role of radiation view factor in thermal performance of straight-fin heat sinks," *International Communications in Heat and Mass Tranfer,* vol. 37, pp. 1087-1095, 2010.

[5] F. K. Moore, "Minimum size of large dry cooling towers with combined mechanical and natural draft," *J. Heat Transfer,* vol. 95, no. 3, 1973.

[6] K. T. Lee and W. M. Yan, "Laminar natural convection between partially heated vertical parallel plates," *Wärme-und Stofföbertragung,* no. 29, 1994.

[7] D. Naylor and J. D. Tarasuk, "Natural convective heat transfer in a divided vertical channel. I: Numerical study.," *Journal of heat transfer,* vol. 2, no. 115, 1993.

[8] D. Naylor and J. D. Tarasuk, "Natural convective heat transfer in a divided vertical channel. II: Experimental study.," *Journal of heat Transfer,* vol. 2, no. 115, 1993.

[9] T. S. Fisher, K. E. Torrance and K. K. Sikka, "Analysis and optimization of a natural draft heat sink system.," *IEEE Transactions on Components, Packaging, and Manufacturing Technology Part A ,* vol. 2, no. 20, 1997.

[10] S. J. Kline and F. A. and McClintock, "Describing uncertainties in single-sample experiments," *Mechanical engineering,* vol. 1, no. 75, 1953.

[11] A. Bar-Cohen and W. M. Rohsenow, "Thermally optimum spacing of vertical, natural convection cooled, parallel plates," in *Heat transfer in electronic equipment*, Washington, 1981.

[12] F. Incropera, D. P. DeWitt, T. L. Bergman and A. S. Lavine, Fundamentals of heat and mass transfer, Hoboken, NJ: John Wiley & Sons, Inc., 2006.

[13] Y. Shabany, Heat Transfer; Thermal Management of Electronics, Boca Raton Florida: Taylor & Francis Group, 2010.

[14] P. H. Oosthuizen, "A numerical study of laminar free convective flow through a vertical open partially heated plane duct," *ASME HTD,* no. 32, 1984.